Hindawi
Mathematical Problems in Engineering
Volume 2018, Article ID 5693618, 13 pages
https://doi.org/10.1155/2018/5693618

Research Article

Dynamics of Nonlinear Primary Oscillator with Nonlinear Energy Sink under Harmonic Excitation: Effects of Nonlinear Stiffness

Min Sun [1] **and Jianen Chen** [2,3]

[1] *School of Science, Tianjin Chengjian University, Tianjin 300384, China*
[2] *Tianjin Key Laboratory of the Design and Intelligent Control of the Advanced Mechatronical System, Tianjin University of Technology, Tianjin 300384, China*
[3] *National Demonstration Center for Experimental Mechanical and Electrical Engineering Education, Tianjin University of Technology, Tianjin 300384, China*

Correspondence should be addressed to Min Sun; sunmin0537@163.com

Received 31 March 2018; Revised 15 July 2018; Accepted 13 August 2018; Published 2 September 2018

Academic Editor: Viktor Avrutin

The dynamics of a system consisting of a nonlinear primary oscillator, subjected to a harmonic external force, and a nonlinear energy sink (NES) are investigated. The analytical solutions for the steady-state responses are obtained by the complexification-averaging method and the analytical model is confirmed by numerical simulations. The results indicate that the introduction of the NES can effectively suppress the vibrations of the primary oscillator. However, as the excitation amplitude increased, the NES may lose its efficiency within certain frequency range due to the appearance of the high response branches. Following the results analysis, it is concluded that this failure can be eliminated by reducing the nonlinear stiffness of the NES properly. The effects of nonlinear stiffness of the primary oscillator on the corresponding responses are also studied. The increase in this nonlinear stiffness can reduce the response amplitude and alter the frequency band where the high branches exist.

1. Introduction

The nonlinear energy sink, consisting of a small mass and a pure nonlinear spring, constitutes an effective solution for vibration suppression over a broad frequency range [1–3]. It can result in a one-way irreversible energy transfer from the primary system to the NES. Compared to traditional linear and weakly nonlinear absorbers, the NES has the higher suppression efficiency under many conditions [4, 5].

The targeted energy transfer (TET) in mechanical systems is one of the attractive issues in the past decades. The introduction of the strong nonlinearity to the primary system can lead to complicated dynamic responses. The mechanisms and phenomena of the nonlinear TET, such as the transient and sustained resonance captures, energy localization, and weakly and strongly modulation responses, were of high concern to researchers [6–8]. Applications of the NES for the vibration suppression in various structures were reported in several papers. Theoretical and experimental studies indicated that the vibrations of beams [9, 10], plates [11, 12], circular cylinders [13], and stay-cables [14] can be effectively suppressed by the NES attachment. With the deepening of research, NES has been applied increasingly to suppress vibration of complicated engineering systems such as rotor-blisk-journal bearing system [15], helicopter [16], and whole-spacecraft [17].

The investigation on energy transfer efficiency of the NES when the primary system is excited by harmonic load is an indispensable part of applications for this absorber [18, 19]. Following a series of optimization, the essentially nonlinear absorber exhibited apparent advantages over linear or weakly nonlinear counterparts. However, a main drawback in NES exists: several unwanted additional branches of response may become apparent under certain conditions. The strategy which can eliminate these branches is a key issue for robust increase of this absorber [20, 21]. In addition, in the vast

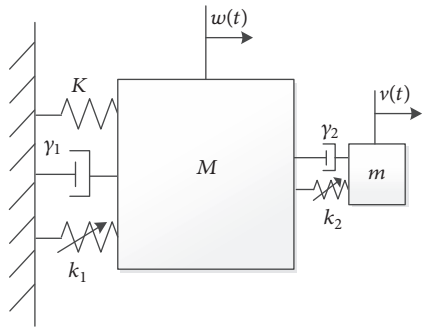

Figure 1: Nonlinear primary oscillator with a nonlinear energy sink.

majority of cases, the controlled primary systems were linear models. These researches contributed significantly to the characteristics of the nonlinear TET. However, many engineering structures present nonlinear characters, and their nonlinear phenomena must be considered [22–25]. The dynamics of the TET system where the nonlinear factors of the primary system were taken into account had been paid more attentions [26–29].

In the current study, the steady-state responses of a nonlinear primary oscillator coupled to a NES are investigated by the complexification-averaging technique. The nonlinear frequency responses of the system under various excitation amplitudes are considered. The nonlinear stiffness of the NES is adjusted to attempt to eliminate these unwanted branches. Also, the effects of the nonlinear stiffness of both the NES and primary oscillator on the vibration suppression are analyzed and compared.

2. Dynamic System

A nonlinear primary oscillator with a single degree of freedom essentially nonlinear attachment is presented in Figure 1. A harmonic external force is imposed on the primary oscillator. The dynamic equation for the integrated system is derived as follows:

$$\ddot{w} + \gamma_1 \dot{w} + Kw + k_1 w^3 + k_2 (w - v)^3 + \gamma_2 (\dot{w} - \dot{v}) = f \cos \Omega t, \tag{1a}$$

$$\varepsilon \ddot{v} + k_2 (v - w)^3 + \gamma_2 (\dot{v} - \dot{w}) = 0, \tag{1b}$$

where K, k_1, and γ_1 are the linear stiffness, nonlinear stiffness, and linear damping of the primary oscillator, respectively. k_2 and γ_2 are the nonlinear stiffness and linear damping of the NES. f and Ω represent the excitation amplitude and frequency, respectively. ε is the mass ratio between the NES and the primary oscillator and $0 < \varepsilon \ll 1$. For convenience, we let $M = 1$.

The complexification-averaging technique is utilized to obtain the slow-flow model of the integrated system, whereas the following transformations are introduced:

$$\begin{aligned} u(t) &= w(t) - v(t), \\ \dot{w} + i\Omega w &= \alpha_1 e^{i\Omega t}, \\ \dot{w} - i\Omega w &= \overline{\alpha}_1 e^{-i\Omega t}, \\ \dot{u} + i\Omega u &= \alpha_2 e^{i\Omega t}, \\ \dot{u} - i\Omega u &= \overline{\alpha}_2 e^{-i\Omega t}, \end{aligned} \tag{2}$$

where $\overline{\alpha}_n$ is the conjugate of the α_n, $(n = 1, 2)$, $i = \sqrt{-1}$. Based on expression (2), we have

$$\begin{aligned} w &= \frac{\alpha_1 e^{i\Omega t} - \overline{\alpha}_1 e^{-i\Omega t}}{2i\Omega}, \\ \dot{w} &= \frac{\alpha_1 e^{i\Omega t} + \overline{\alpha}_1 e^{-i\Omega t}}{2}, \\ \ddot{w} &= \frac{1}{2}\left(\dot{\alpha}_1 e^{i\Omega t} + i\Omega \alpha_1 e^{i\Omega t} + \dot{\overline{\alpha}}_1 e^{-i\Omega t} - i\Omega \overline{\alpha}_1 e^{-i\Omega t}\right), \\ u &= \frac{\alpha_2 e^{i\Omega t} - \overline{\alpha}_2 e^{-i\Omega t}}{2i\Omega}, \\ \dot{u} &= \frac{\alpha_2 e^{i\Omega t} + \overline{\alpha}_2 e^{-i\Omega t}}{2}, \\ \ddot{u} &= \frac{1}{2}\left(\dot{\alpha}_2 e^{i\Omega t} + i\Omega \alpha_2 e^{i\Omega t} + \dot{\overline{\alpha}}_2 e^{-i\Omega t} - i\Omega \overline{\alpha}_2 e^{-i\Omega t}\right). \end{aligned} \tag{3}$$

Substituting (3) into (1a) and (1b) and retaining the slow-flow parts, we obtain

$$\dot{\alpha}_1 + i\Omega \alpha_1 + \gamma_1 \alpha_1 + \frac{K\alpha_1}{i\Omega} + \frac{3k_1 \alpha_1^2 \overline{\alpha}_1}{4i\Omega^3} + \frac{3k_2 \alpha_2^2 \overline{\alpha}_2}{4i\Omega^3} + \gamma_2 \alpha_2 = f, \tag{4a}$$

$$\varepsilon\left(\dot{\alpha}_1 + i\Omega \alpha_1 - \dot{\alpha}_2 - i\Omega \alpha_2\right) - \frac{3k_2 \alpha_2^2 \overline{\alpha}_2}{4i\Omega^3} - \gamma_2 \alpha_2 = 0. \tag{4b}$$

Letting,

$$\begin{aligned} \alpha_1 &= a_1 + ib_1, \\ \alpha_2 &= a_2 + ib_2. \end{aligned} \tag{5}$$

We substitute (5) into (4a) and (4b) and separate real and imaginary parts, yielding

$$\dot{a}_1 = -a_1\gamma_1 + b_1\Omega - \frac{Kb_1}{\Omega} - \frac{3k_2b_2\left(a_2^2+b_2^2\right)}{4\Omega^3} - \gamma_2 a_2 - \frac{3k_1b_1\left(a_1^2+b_1^2\right)}{4\Omega^3} + f, \tag{6a}$$

$$\dot{b}_1 = -a_1\Omega - b_1\gamma_1 + \frac{Ka_1}{\Omega} + \frac{3k_2a_2\left(a_2^2+b_2^2\right)}{4\Omega^3} - \gamma_2 b_2 + \frac{3k_1a_1\left(a_1^2+b_1^2\right)}{4\Omega^3}, \tag{6b}$$

$$\varepsilon\dot{a}_2 - \varepsilon\dot{a}_1 = \varepsilon\Omega b_2 - \varepsilon\Omega b_1 - \frac{3k_2b_2\left(a_2^2+b_2^2\right)}{4\Omega^3} - \gamma_2 a_2, \tag{6c}$$

$$\varepsilon\dot{b}_2 - \varepsilon\dot{b}_1 = \varepsilon\Omega a_1 - \varepsilon\Omega a_2 + \frac{3k_2a_2\left(a_2^2+b_2^2\right)}{4\Omega^3} - \gamma_2 b_2. \tag{6d}$$

The steady-state responses of the system are investigated through letting $\dot{a}_1 = 0$, $\dot{b}_1 = 0$, $\dot{a}_2 = 0$, $\dot{b}_2 = 0$. Solving the resulting nonlinear algebraic equations, the response amplitude of the primary oscillator and the relative motion between two oscillators are obtained and the expressions are, respectively,

$$w = \frac{\sqrt{a_1^2+b_1^2}}{\Omega}, \qquad w - v = \frac{\sqrt{a_2^2+b_2^2}}{\Omega}. \tag{7}$$

In order for the stability of the steady-state solutions to be analyzed, the small perturbations δ_n $(n = 1, 2, 3, 4)$ are introduced:

$$a_1 = a_{10} + \delta_1, \quad b_1 = b_{10} + \delta_2, \quad a_2 = a_{20} + \delta_3, \quad b_2 = b_{20} + \delta_4, \tag{8}$$

where a_{10}, b_{10}, a_{20}, b_{20} are the steady-state solutions of the system. Substituting (8) into (6a), (6b), (6c), and (6d) yields

$$\dot{\delta}_1 = -\gamma_1\delta_1 + \Omega\delta_2 - \frac{K}{\Omega}\delta_2 - \frac{3k_2}{4\Omega^3}\left[\left(a_{20}^2+3b_{20}^2\right)\delta_4 + 2a_{20}b_{20}\delta_3\right] - \gamma_2\delta_3 - \frac{3k_1}{4\Omega^3}\left[\left(a_{10}^2+3b_{10}^2\right)\delta_2 + 2a_{10}b_{10}\delta_1\right], \tag{9a}$$

$$\dot{\delta}_2 = -\gamma_1\delta_2 - \Omega\delta_1 + \frac{K}{\Omega}\delta_1 + \frac{3k_2}{4\Omega^3}\left[\left(3a_{20}^2+b_{20}^2\right)\delta_3 + 2a_{20}b_{20}\delta_4\right] - \gamma_2\delta_4 + \frac{3k_1}{4\Omega^3}\left[\left(3a_{10}^2+b_{10}^2\right)\delta_1 + 2a_{10}b_{10}\delta_2\right], \tag{9b}$$

$$\dot{\delta}_3 = \Omega\delta_4 - \Omega\delta_2 - \frac{3k_2}{4\varepsilon\Omega^3}\left[\left(a_{20}^2+3b_{20}^2\right)\delta_4 + 2a_{20}b_{20}\delta_3\right] - \frac{\gamma_2\delta_3}{\varepsilon} + \dot{\delta}_1, \tag{9c}$$

$$\dot{\delta}_4 = \Omega\delta_1 - \Omega\delta_3 + \frac{3k_2}{4\varepsilon\Omega^3}\left[\left(3a_{20}^2+b_{20}^2\right)\delta_3 + 2a_{20}b_{20}\delta_4\right] - \frac{\gamma_2\delta_4}{\varepsilon} + \dot{\delta}_2. \tag{9d}$$

The coefficient matrix of (9a), (9b), (9c), and (9d) is presented as follows; the eigenvalues of the matrix can be used to determine the stability of the solutions:

$$J = \begin{pmatrix} J_{11} & J_{12} & J_{13} & J_{14} \\ J_{21} & J_{22} & J_{23} & J_{24} \\ J_{31} & J_{32} & J_{33} & J_{34} \\ J_{41} & J_{42} & J_{43} & J_{44} \end{pmatrix}, \tag{10}$$

where

$$J_{11} = -\gamma_1 - \frac{3k_1a_{10}b_{10}}{2\Omega^3}, \quad J_{12} = \Omega - \frac{K}{\Omega} - \frac{3k_1\left(a_{10}^2+3b_{10}^2\right)}{4\Omega^3}, \quad J_{13} = -\gamma_2 - \frac{3k_2a_{20}b_{20}}{2\Omega^3}, \quad J_{14} = -\frac{3k_2\left(a_{20}^2+3b_{20}^2\right)}{4\Omega^3},$$

$$J_{21} = -\Omega + \frac{K}{\Omega} + \frac{3k_1\left(3a_{10}^2+b_{10}^2\right)}{4\Omega^3}, \quad J_{22} = -\gamma_1 + \frac{3k_1a_{10}b_{10}}{2\Omega^3}, \quad J_{23} = \frac{3k_2\left(3a_{20}^2+b_{20}^2\right)}{4\Omega^3}, \quad J_{24} = -\gamma_2 + \frac{3k_2a_{20}b_{20}}{2\Omega^3},$$

$$J_{31} = -\gamma_1 - \frac{3k_1a_{10}b_{10}}{2\Omega^3},$$

$$
\begin{aligned}
J_{32} &= -\frac{K}{\Omega} - \frac{3k_1\left(a_{10}^2 + 3b_{10}^2\right)}{4\Omega^3},\\
J_{33} &= -\frac{\gamma_2}{\varepsilon} - \frac{3k_2a_{20}b_{20}}{2\varepsilon\Omega^3} - \gamma_2 - \frac{3k_2a_{20}b_{20}}{2\Omega^3},\\
J_{34} &= \Omega - \frac{3k_2\left(a_{20}^2 + 3b_{20}^2\right)}{4\varepsilon\Omega^3} - \frac{3k_2\left(a_{20}^2 + 3b_{20}^2\right)}{4\Omega^3},\\
J_{41} &= \frac{K}{\Omega} + \frac{3k_1\left(3a_{10}^2 + b_{10}^2\right)}{4\Omega^3},\\
J_{42} &= -\gamma_1 + \frac{3k_1a_{10}b_{10}}{2\Omega^3},\\
J_{43} &= -\Omega + \frac{3k_2\left(3a_{20}^2 + b_{20}^2\right)}{4\varepsilon\Omega^3} + \frac{3k_2\left(3a_{20}^2 + b_{20}^2\right)}{4\Omega^3},\\
J_{44} &= -\frac{\gamma_2}{\varepsilon} + \frac{3k_2a_{20}b_{20}}{2\varepsilon\Omega^3} - \gamma_2 + \frac{3k_2a_{20}b_{20}}{2\Omega^3}.
\end{aligned}
\tag{11}
$$

3. Validation

The numerical results are utilized for the predictions confirmation of the analytical model. The Runge-Kutta method is directly attacking (1a) and (1b) to obtain the numerical results. It is demonstrated in Figure 2(a) that the results obtained from these two methods agree well. In Figure 2(a), squares and circles represent stable and unstable solutions obtained from complexification-averaging technique, respectively. Pluses represent numerical solutions obtained from Runge-Kutta method. Moreover, the stability of the analytical results is also presented in this figure. In order for the general applicability of the results to be ensured, all parameters in (1a) and (1b) are dimensionless values. The stable responses when $\Omega = 14.8$ and $\Omega = 15.7$ as well as the unstable responses when $\Omega = 15.1$ and $\Omega = 15.4$ are shown in Figures 2(b)–2(e), respectively. The unstable responses demonstrate a kind of relaxation oscillation, usually referred to as strong modulation response. These parameters are selected, respectively, as $K = 225$, $k_1 = 50$, $k_2 = 700$, $\gamma_1 = 0.1$, $\gamma_2 = 0.2$, $\varepsilon = 0.1$, $f = 1$.

4. Results and Discussions

4.1. Effects of NES Nonlinear Stiffness. The vibration suppression efficiency is of most concern. In this section, the efficiency is investigated under various harmonic excitation amplitudes by the analytical method, whereas all parameters except the nonlinear stiffness k_2 are selected as the parameters in Section 3. Figure 3 illustrates the nonlinear frequency responses of the primary oscillator without the NES and with various NESs under $f = 1$. When the nonlinear stiffness k_2 is selected as 100, the good vibration suppression effect is achieved, the value of the resonance peak is reduced exceeding three times with respect to that of the primary oscillator without the NES attached. In this case, the responses in the entire frequency band are stable. When the nonlinear stiffness k_2 is increased to 400, the unstable responses appear approximately at $\Omega = 15$ and the suppression efficiency of this NES is enhanced compared to that of the NES with $k_2 = 100$. Generally, the weakly/strongly modulation responses are preferable for vibration suppression. When $k_2 = 700$, the efficiency is further enhanced and the frequency band where the unstable response occurs is broadened. When $k_2 = 1000$, two high branches of the frequency response curve appear in the frequency band [13.4, 14], one is stable and the other is unstable. The appearance of the high stable branch is interpreted that the NES intensifies the vibration of the primary oscillator in this frequency band. When $k_2 = 1300$, compared to those demonstrated in Figure 3(e), the frequency band where the high stable branch exists is broadened and the maximum response amplitude is larger.

The frequency responses of the primary oscillator under the harmonic excitation amplitude $f = 3$ are presented in Figure 4. When $k_2 = 50$, the unstable response appears approximately at $\Omega = 15$ and a large amount of vibration energy is dissipated. When $k_2 = 150$ and $k_2 = 250$, the high branches appear, whereas the frequency band where the high stable branch appears to be broader as the nonlinear stiffness increased. When the excitation amplitude $f = 5$, the variations in the frequency response along with the nonlinear stiffness k_2 are the same as those demonstrated in Figures 3 and 4. It is noted that the high branches appear as $k_2 = 50$ in this case. Comparing Figures 3–5, it is discovered that, prior to the appearance of the high response branches, the unstable response occurs approximately at the linear natural frequency of the primary oscillator firstly. In addition, as the excitation amplitude increased, the lower stiffness should be selected to prevent the appearance of the high branches of the frequency response.

Then, the bifurcations for the primary oscillator via the nonlinear stiffness of the NES under a fixed excitation frequency and various excitation amplitudes are studied. When $\Omega = 15$, the response amplitude always remains at the relatively low value as $f = 2$ in the studied value range of the nonlinear stiffness. As the excitation amplitude increased, the high branches will appear at certain stiffness. For example, when $f = 3$, the response amplitude decreases with increasing the nonlinear stiffness k_2 at first, and the response of the primary oscillator becomes unstable as $k_2 = 93$. Next, the high branches of the response amplitude appear until the nonlinear stiffness $k_2 = 147$. Comparing the four subfigures in Figure 6, it is worth being noted that the larger the excitation amplitude, the lower the stiffness which corresponds to the bifurcation point. Figure 7 shows that, when $\Omega = 15.5$, the response amplitude always remains the relatively lower value as $f = 2$; however, a bifurcation occurs as the nonlinear stiffness $k_2 = 93$ and the response becomes unstable after the nonlinear stiffness $k_2 = 132$. Similarly, the stiffness which corresponds to the bifurcation point is reduced as the excitation amplitude increased.

4.2. Effects of Primary Oscillator Nonlinear Stiffness. The effects of the primary oscillator nonlinear stiffness on the frequency response are investigated. All parameters except k_1

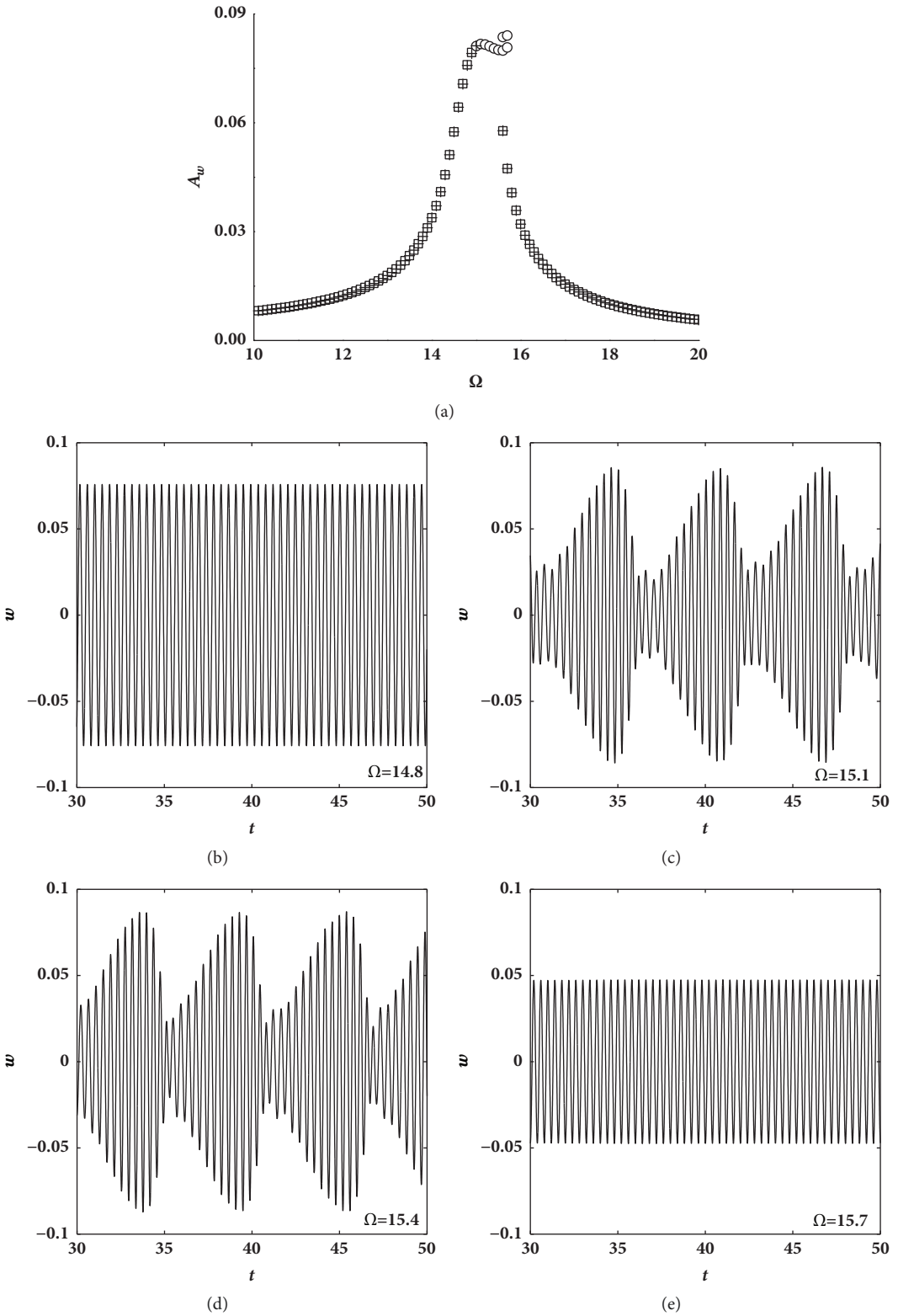

Figure 2: Analytical model validation.

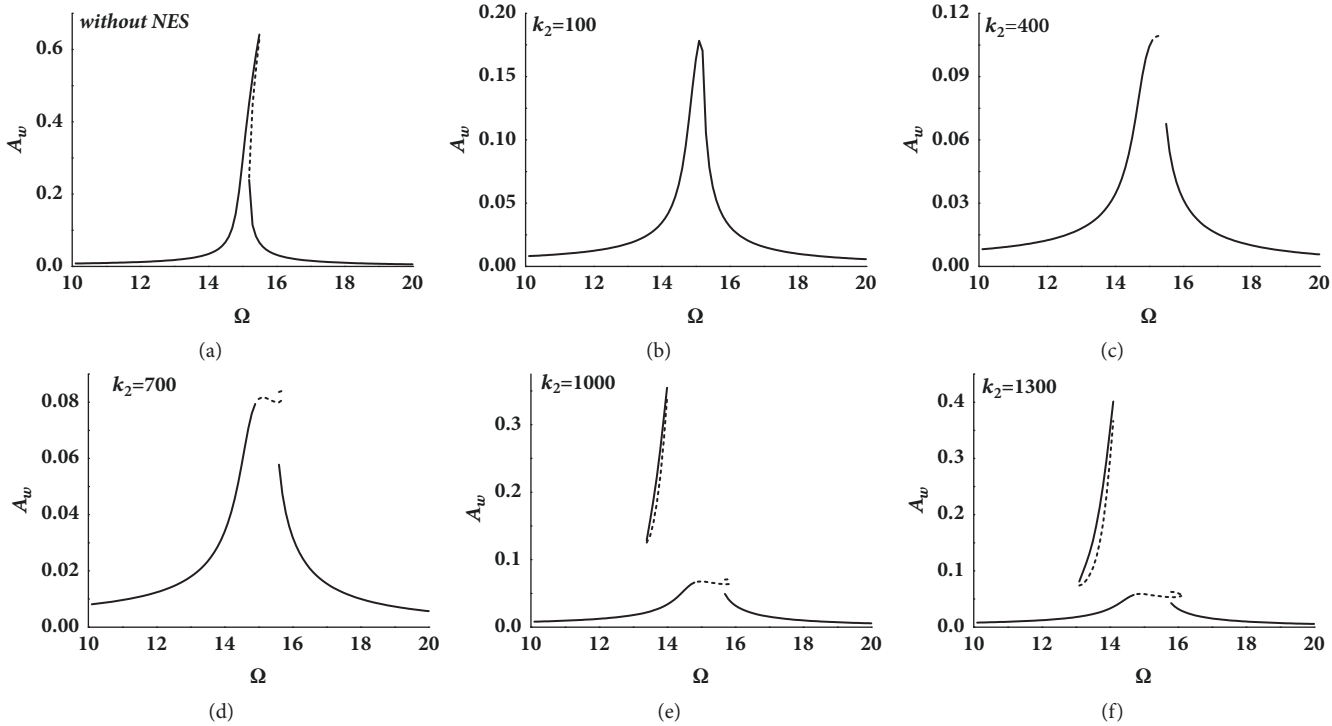

Figure 3: Frequency responses of the primary oscillator with various NESs as $f = 1$ and $k_1 = 50$.

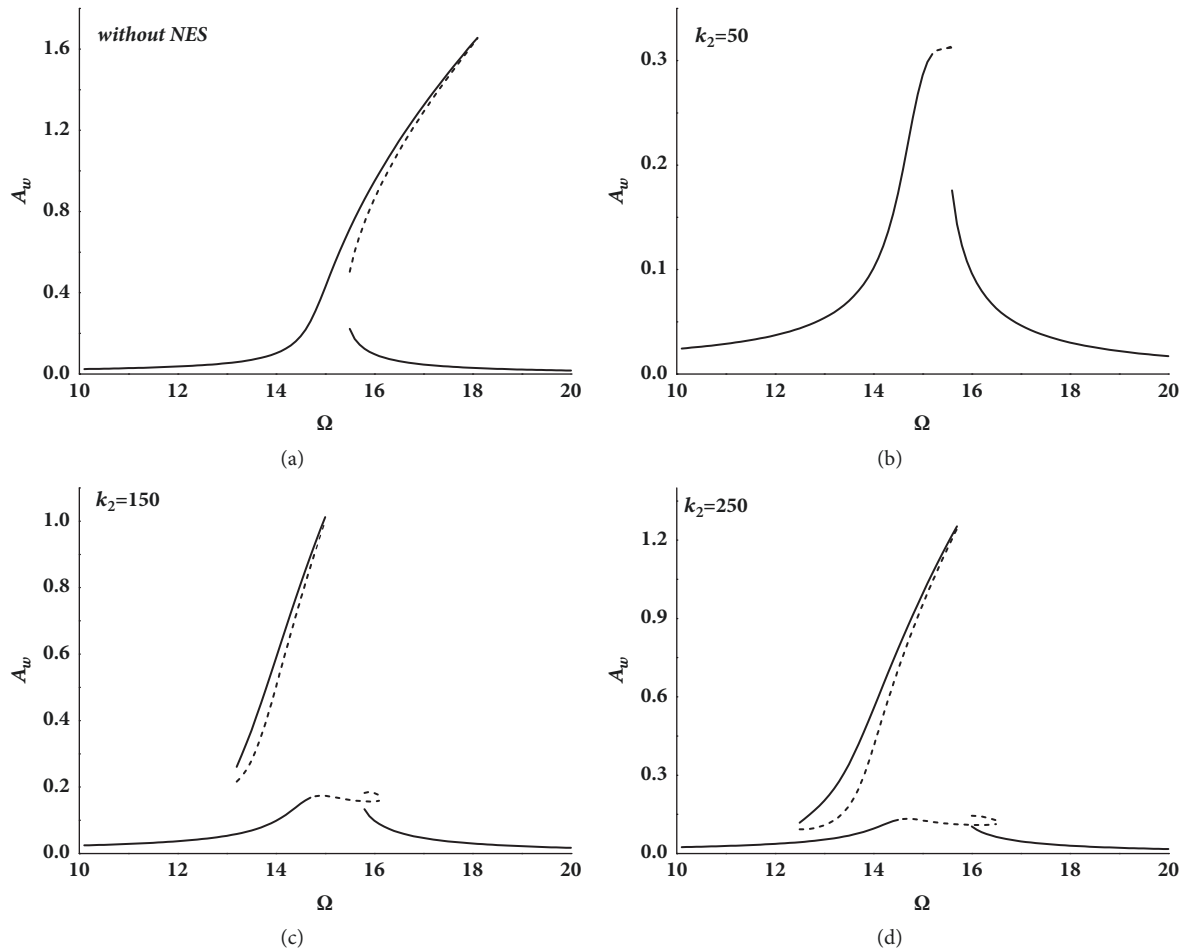

Figure 4: Frequency responses of the primary oscillator with various NESs as $f = 3$ and $k_1 = 50$.

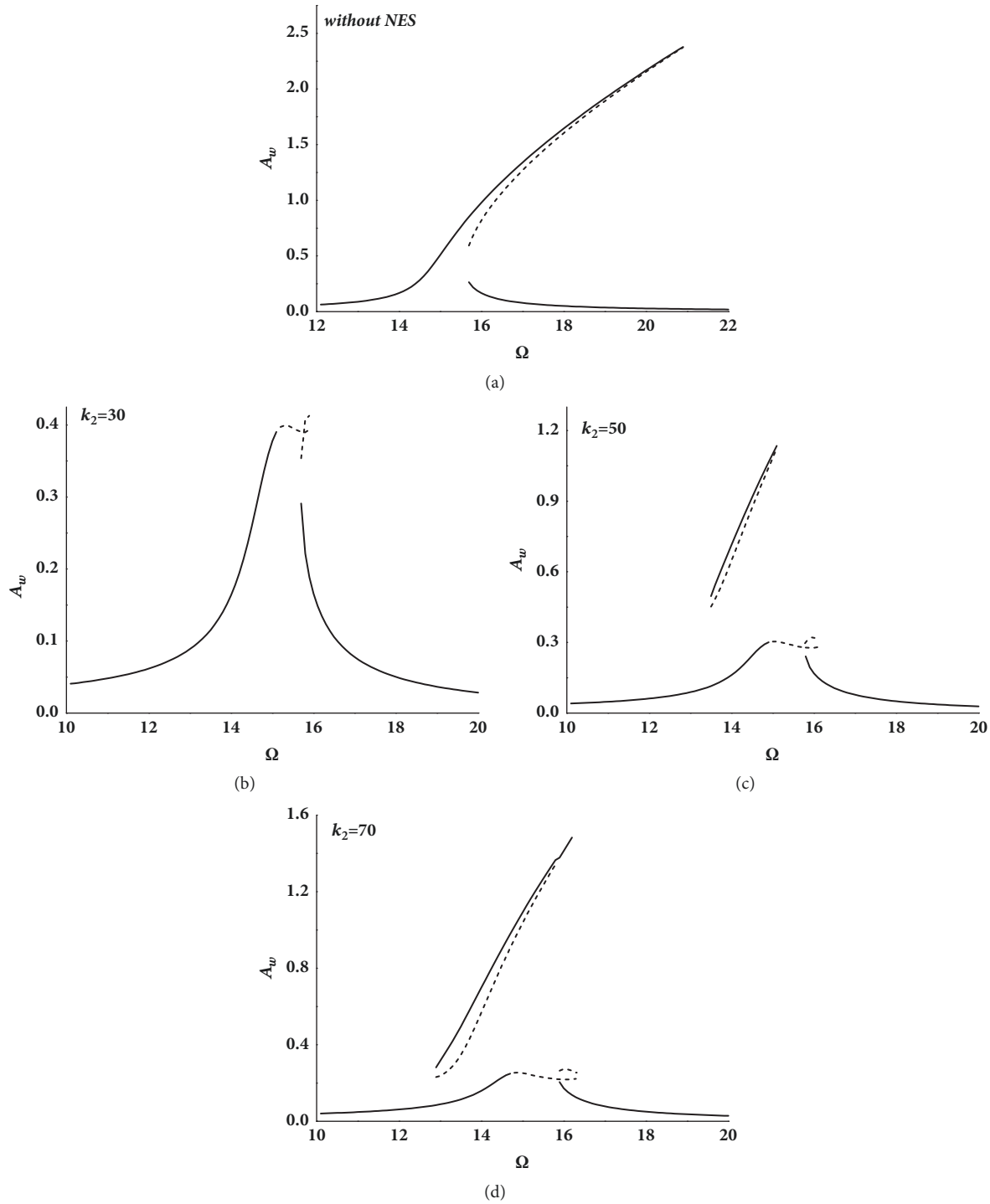

Figure 5: Frequency responses of the primary oscillator with various NESs as $f = 5$ and $k_1 = 50$.

and k_2 are the same as those in Figure 4. Figure 8 is depicted as $k_1 = 0$ (i.e., the primary oscillator is linear). The change rates of the response amplitude, within the high stable branches in Figures 8(c) and 8(d), are quite different from the counterparts when $k_1 \neq 0$. Comparing the responses of the primary oscillator without the NES, which are demonstrated in Figures 4(a), 8(a), 9(a), and 10(a), it is indicated that the value of the resonance peak decreases and the frequency which corresponds to the resonance peak increases with the raise of the nonlinear stiffness k_1. It can also be concluded by comparing the rest figures in Figures 4, 9, and 10 that the integrated systems with the various values of k_1 and the same value of k_2 have the similar response. Similar to the effects of the nonlinear stiffness k_1 on the dynamics

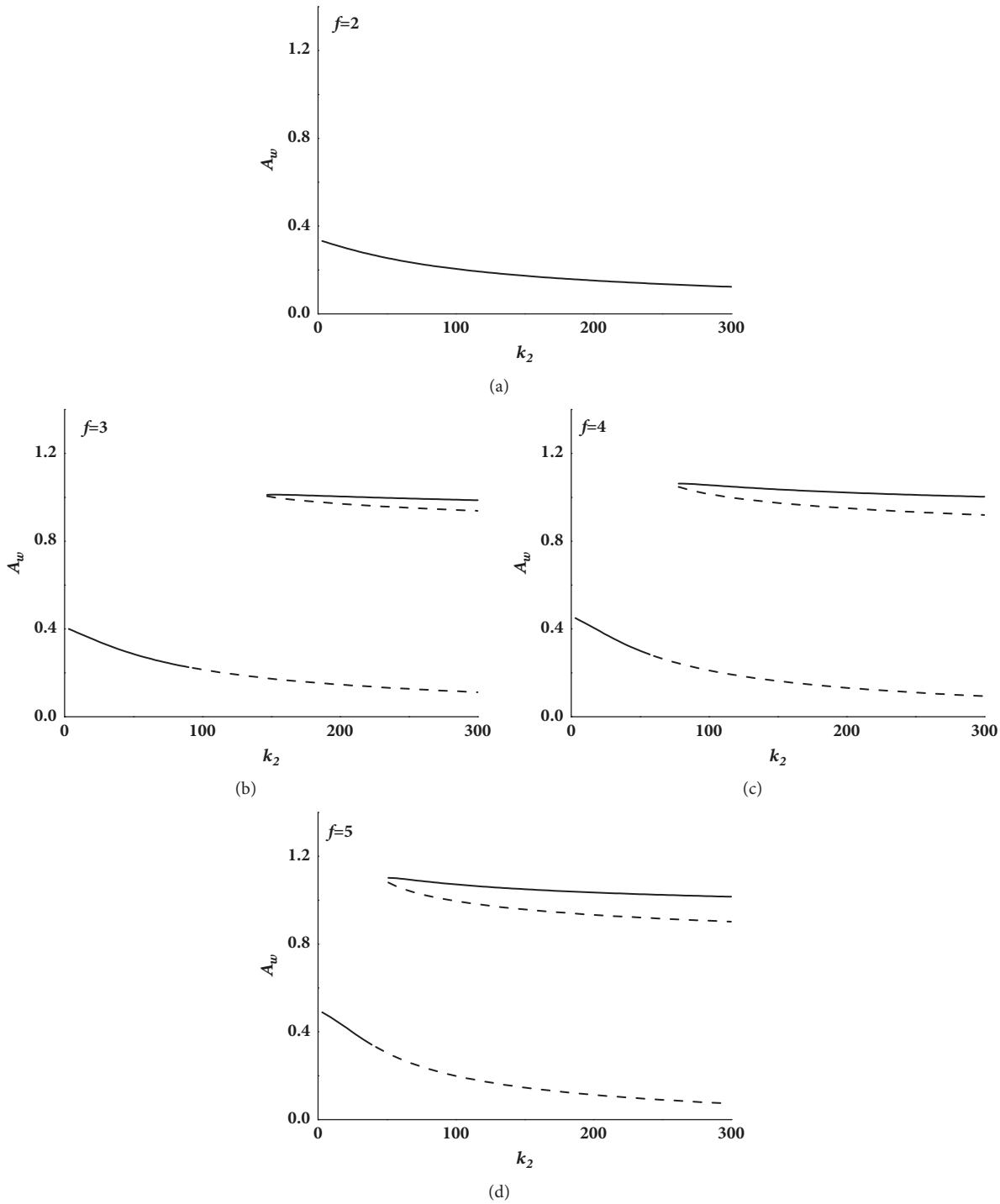

Figure 6: Bifurcations of primary oscillator as $\Omega = 15$.

of the primary oscillator without the NES, an increase in the nonlinear stiffness k_1 brings about the decrease of the unwanted branches when the NES is coupled to the primary oscillator. In addition, the nonlinear stiffness k_1 has a small effect on the frequency range of the high branches of the frequency response.

5. Concluding Remarks

The effects of the nonlinear stiffness of both the NES and primary oscillator on the dynamics of the primary oscillator under various harmonic excitations are investigated. The complexification-averaging technique is utilized to obtain the

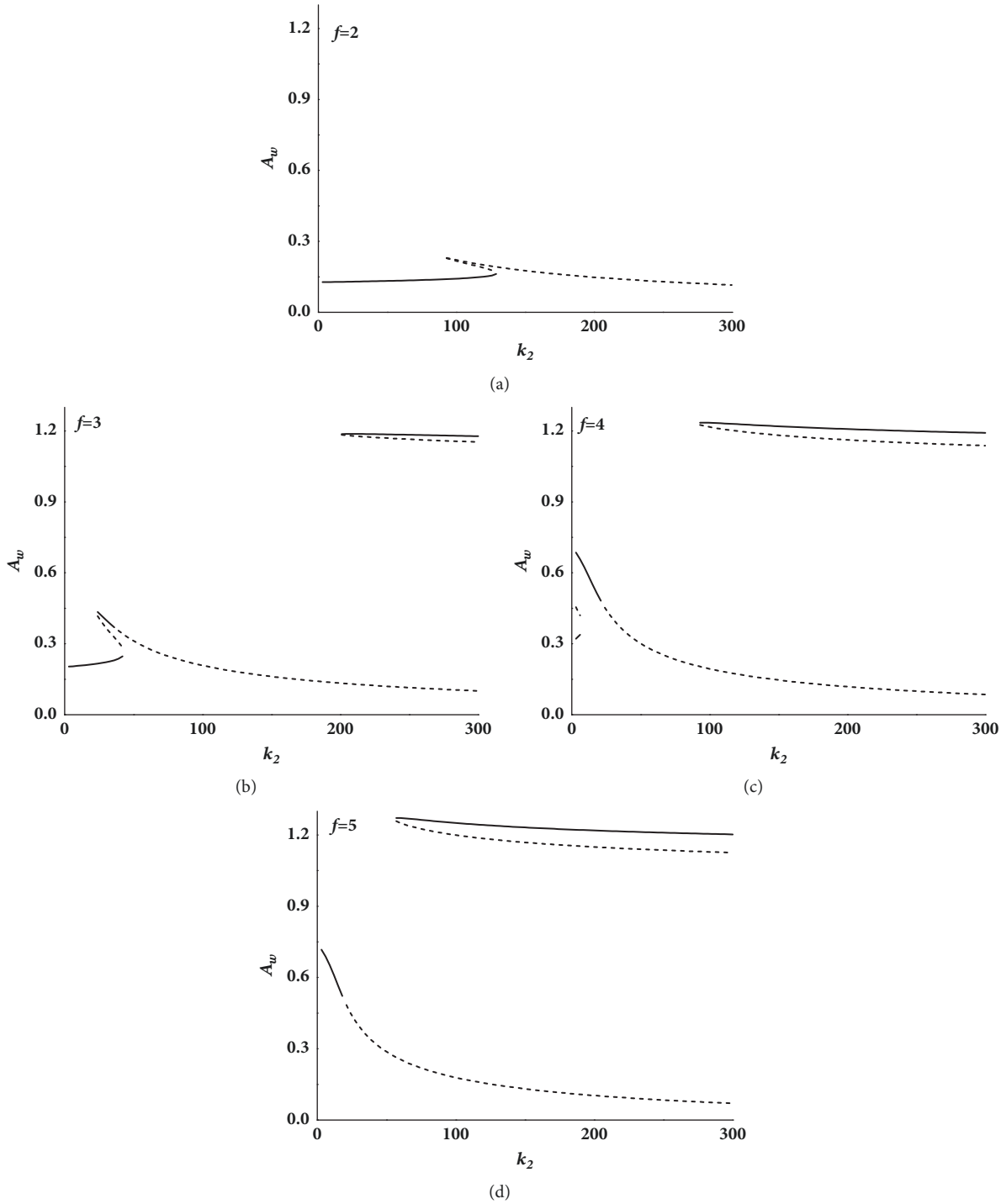

Figure 7: Bifurcations of primary oscillator as $\Omega = 15.5$.

analytical model of the integrated system, and the coefficient matrix of the integrated system with small perturbation is obtained to analyze the stability of the dynamic responses.

The predictions of the analytical model are confirmed by numerical simulations. The analytical results demonstrate that the vibration suppression can be enhanced by increasing the NES nonlinear stiffness. However, the high branches appear following the stiffness excessive increase. As the stiffness remains fixed, the high branches also can appear with the excitation amplitude increases. Actually, for preventing the appearance of the high branches of the frequency response under the large amplitude external force, the nonlinear stiffness should be properly adjusted to a relatively low value. Therefore, the utilization of a semiactive control is an efficient

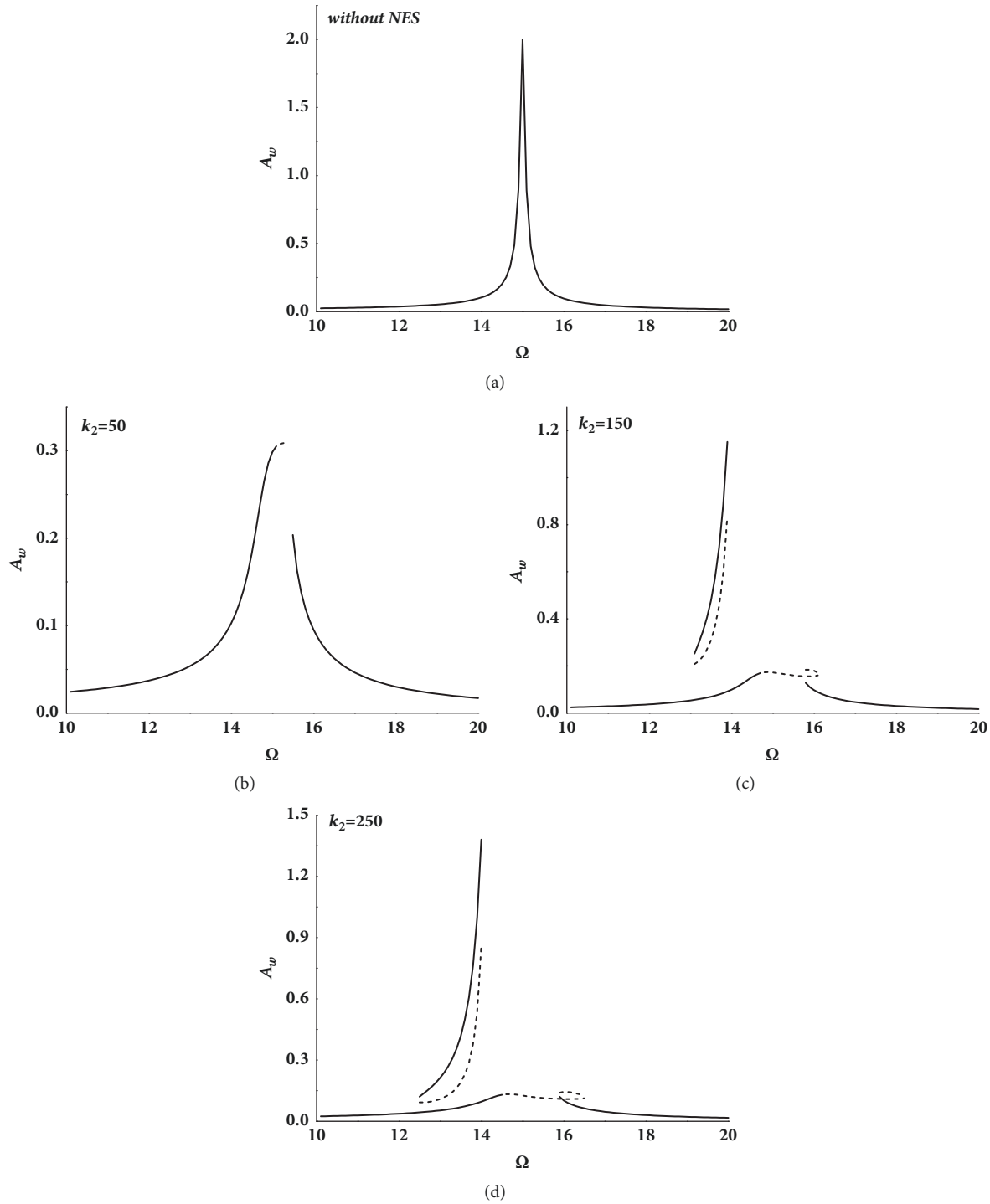

Figure 8: Frequency responses of the linear primary oscillator with various NESs as $f = 3$.

method for the robustness improvement of the nonlinear absorber.

The NES brings an extra nonlinear factor to the nonlinear primary oscillator. A distinction should be made between the contributions of the two nonlinear factors. The results indicate that the introduction of the strongly nonlinear factor can not only suppress the vibrations of the primary oscillator but also can result in the bifurcations and instability of the responses under certain conditions. In the system studied in this paper, by contrast, the effects of the nonlinear stiffness of the primary oscillator are relatively simple. The increase in this nonlinear stiffness can reduce the response amplitude and alter the frequency band where the high branches exist. Also, the stiffness of the primary oscillator can affect the

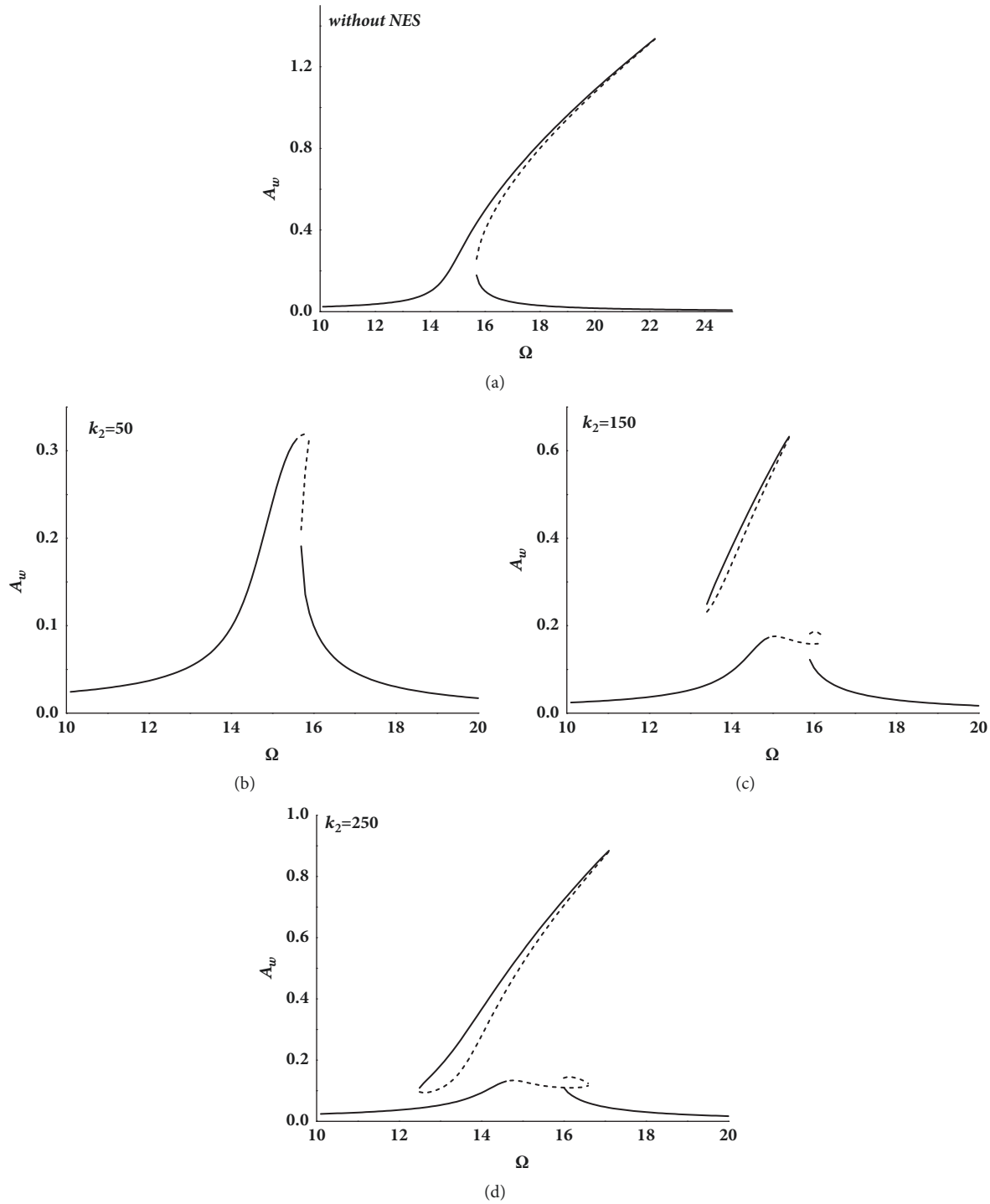

Figure 9: Frequency responses of the primary oscillator with various NESs as $k_1 = 200$ and $f = 3$.

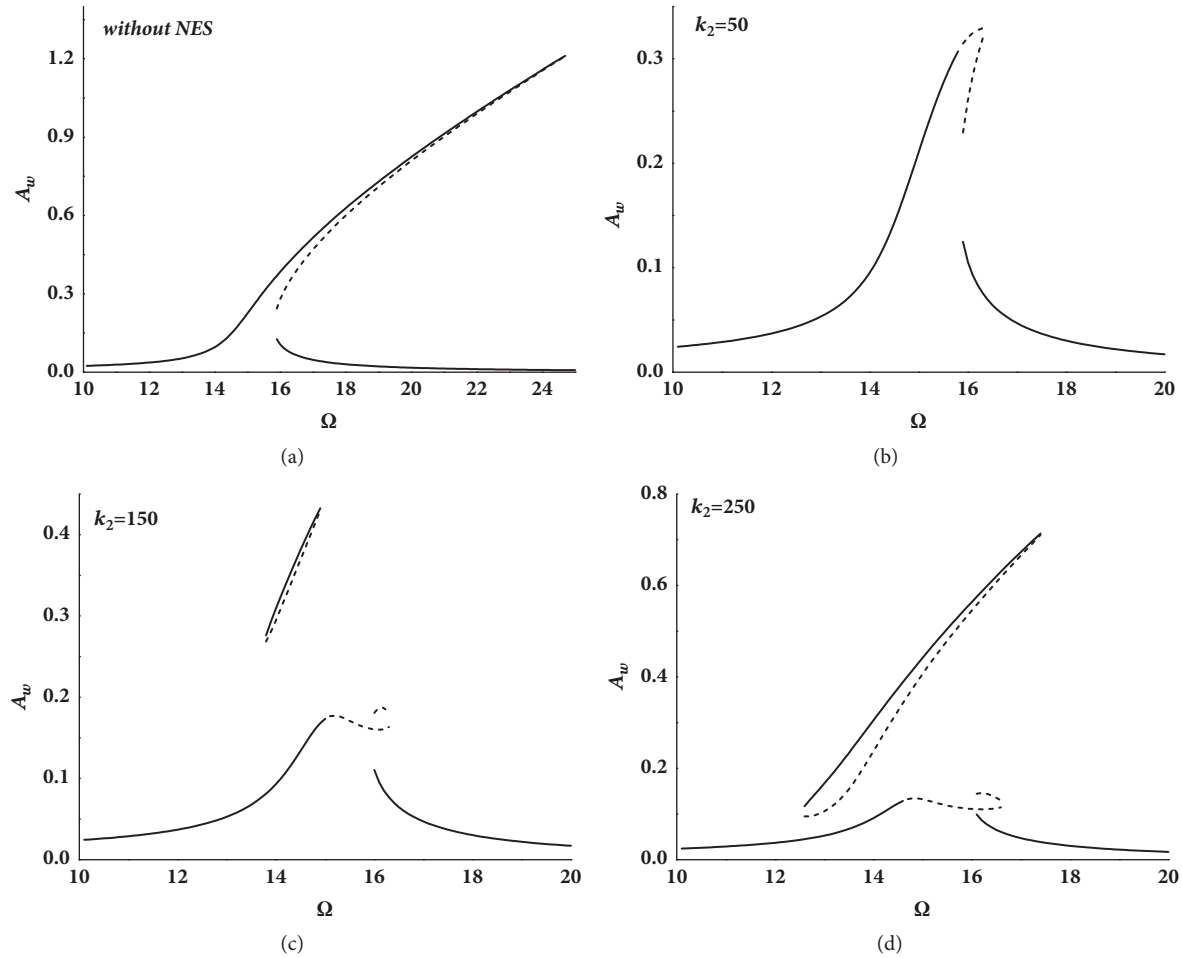

Figure 10: Frequency responses of the primary oscillator with various NESs as $k_1 = 350$ and $f = 3$.

value of the NES optimal stiffness. In this work, the cubic nonlinearity of the primary oscillator is considered only. The effects of the NES on the dynamics of the primary oscillator which has more complex nonlinear factors are required to be further investigated.

Data Availability

The datasets used during the current study are available from the corresponding author on reasonable request.

Conflicts of Interest

The authors declare that they have no conflicts of interest.

Acknowledgments

This research was supported by the National Natural Science Foundation of China (nos. 11402165 and 11402170) and Tianjin Natural Science Foundation of China (no. 17JCYBJC18800).

References

[1] O. V. Gendelman, "Transition of energy to a nonlinear localized mode in a highly asymmetric system of two oscillators," *Nonlinear Dynamics*, vol. 25, pp. 237–253, 2001.

[2] G. Kerschen, Y. S. Lee, A. F. Vakakis, D. M. McFarland, and L. A. Bergman, "Irreversible passive energy transfer in coupled oscillators with essential nonlinearity," *SIAM Journal on Applied Mathematics*, vol. 66, no. 2, pp. 648–679, 2005.

[3] A. F. Vakakis, O. V. Gendelman, L. A. Bergman, D. M. McFarland, G. Kerschen, and Y. S. Lee, *Nonlinear Targeted Energy Transfer in Mechanical and Structural Systems*, Springer, Berlin, Germany, 2009.

[4] A. Tripathi, P. Grover, and T. Kalmár-Nagy, "On optimal performance of nonlinear energy sinks in multiple-degree-of-freedom systems," *Journal of Sound and Vibration*, vol. 388, pp. 272–297, 2017.

[5] F. S. Samani and F. Pellicano, "Vibration reduction on beams subjected to moving loads using linear and nonlinear dynamic absorbers," *Journal of Sound and Vibration*, vol. 325, no. 4-5, pp. 742–754, 2009.

[6] G. Kerschen, J. J. Kowtko, D. McFarland, L. A. Bergman, and A. F. Vakakis, "Theoretical and experimental study of multimodal targeted energy transfer in a system of coupled oscillators," *Nonlinear Dynamics*, vol. 47, pp. 285–309, 2007.

[7] E. Gourdon, C. H. Lamarque, and S. Pernot, "Contribution to efficiency of irreversible passive energy pumping with a strong nonlinear attachment," *Nonlinear Dynamics*, vol. 50, no. 4, pp. 793–808, 2007.

[8] D. D. Quinn, O. Gendelman, G. Kerschen, T. P. Sapsis, L. A. Bergman, and A. F. Vakakis, "Efficiency of targeted energy transfers in coupled nonlinear oscillators associated with 1:1 resonance captures: Part I," *Journal of Sound and Vibration*, vol. 311, no. 3-5, pp. 1228–1248, 2008.

[9] Y.-W. Zhang, Z. Zhang, L.-Q. Chen, T.-Z. Yang, B. Fang, and J. Zang, "Impulse-induced vibration suppression of an axially moving beam with parallel nonlinear energy sinks," *Nonlinear Dynamics*, vol. 82, no. 1-2, pp. 61–71, 2015.

[10] M. Kani, S. E. Khadem, M. H. Pashaei, and M. Dardel, "Design and performance analysis of a nonlinear energy sink attached to a beam with different support conditions," *Proceedings of the Institution of Mechanical Engineers, Part C: Journal of Mechanical Engineering Science*, vol. 230, no. 4, pp. 527–542, 2016.

[11] Y.-W. Zhang, H. Zhang, S. Hou, K.-F. Xu, and L.-Q. Chen, "Vibration suppression of composite laminated plate with nonlinear energy sink," *Acta Astronautica*, vol. 123, pp. 109–115, 2016.

[12] J. E. Chen, W. Zhang, M. H. Yao, J. Liu, and M. Sun, "Vibration reduction in truss core sandwich plate with internal nonlinear energy sink," *Composite Structures*, vol. 193, pp. 180–188, 2018.

[13] H. L. Dai, A. Abdelkefi, and L. Wang, "Vortex-induced vibrations mitigation through a nonlinear energy sink," *Communications in Nonlinear Science and Numerical Simulation*, vol. 42, pp. 22–36, 2017.

[14] M. Izzi, L. Caracoglia, and S. Noè, "Investigating the use of Targeted-Energy-Transfer devices for stay-cable vibration mitigation," *Structural Control and Health Monitoring*, vol. 23, no. 2, pp. 315–332, 2016.

[15] S. Bab, S. E. Khadem, M. Shahgholi, and A. Abbasi, "Vibration attenuation of a continuous rotor-blisk-journal bearing system employing smooth nonlinear energy sinks," *Mechanical Systems and Signal Processing*, vol. 84, pp. 128–157, 2017.

[16] B. Bergeot, S. Bellizzi, and B. Cochelin, "Passive suppression of helicopter ground resonance using nonlinear energy sinks attached on the helicopter blades," *Journal of Sound and Vibration*, vol. 392, pp. 41–55, 2017.

[17] K. Yang, Y. W. Zhang, H. Ding, and L. Q. Chen, "Nonlinear energy sink for whole-spacecraft vibration reduction," *Journal of Vibration and Acoustics*, vol. 139, 2017.

[18] J. Zang and L.-Q. Chen, "Complex dynamics of a harmonically excited structure coupled with a nonlinear energy sink," *Acta Mechanica Sinica*, vol. 33, no. 4, pp. 801–822, 2017.

[19] J. E. Chen, W. He, W. Zhang, M. H. Yao, J. Liu, and M. Sun, "Vibration suppression and higher branch responses of beam with parallel nonlinear energy sinks," *Nonlinear Dynamics*, vol. 91, no. 2, pp. 885–904, 2018.

[20] Y. Starosvetsky and O. V. Gendelman, "Attractors of harmonically forced linear oscillator with attached nonlinear energy sink II: Optimization of a nonlinear vibration absorber," *Nonlinear Dynamics*, vol. 51, no. 1-2, pp. 47–57, 2008.

[21] Y. Starosvetsky and O. V. Gendelman, "Vibration absorption in systems with a nonlinear energy sink: Nonlinear damping," *Journal of Sound and Vibration*, vol. 324, no. 3-5, pp. 916–939, 2009.

[22] A. H. Nayfeh and D. T. Mook, *Nonlinear Oscillations*, John Wiley & Sons, New York, NY, USA, 1979.

[23] W. Zhang, "Global and chaotic dynamics for a parametrically excited thin plate," *Journal of Sound and Vibration*, vol. 239, no. 5, pp. 1013–1036, 2001.

[24] W. Zhang, Y. X. Hao, and J. Yang, "Nonlinear dynamics of FGM circular cylindrical shell with clamped-clamped edges," *Composite Structures*, vol. 94, no. 3, pp. 1075–1086, 2012.

[25] R. Q. Wu, W. Zhang, and M. H. Yao, "Nonlinear dynamics near resonances of a rotor-active magnetic bearings system with 16-pole legs and time varying stiffness," *Mechanical Systems and Signal Processing*, vol. 100, pp. 113–134, 2018.

[26] R. Viguié and G. Kerschen, "Nonlinear vibration absorber coupled to a nonlinear primary system: a tuning methodology," *Journal of Sound and Vibration*, vol. 326, no. 3–5, pp. 780–793, 2009.

[27] R. Viguié, M. Peeters, G. Kerschen, and J.-C. Golinval, "Energy transfer and dissipation in a duffing oscillator coupled to a nonlinear attachment," *Journal of Computational and Nonlinear Dynamics*, vol. 4, 2009.

[28] M. Kani, S. E. Khadem, M. H. Pashaei, and M. Dardel, "Vibration control of a nonlinear beam with a nonlinear energy sink," *Nonlinear Dynamics*, vol. 83, no. 1, pp. 1–22, 2016.

[29] M. Parseh, M. Dardel, M. H. Ghasemi, and M. H. Pashaei, "Steady state dynamics of a non-linear beam coupled to a nonlinear energy sink," *International Journal of Non-Linear Mechanics*, vol. 79, pp. 48–65, 2016.